Composites Part B 222 (2021) 109094

Contents lists available at ScienceDirect

Composites Part B

journal homepage: www.elsevier.com/locate/compositesb

Improving the high-cycle fatigue strength of heterogeneous carbon nanotube/Al-Cu-Mg composites through grain size design in ductile-zones

K. Ma [a,b], X.N. Li [a], K. Liu [b], X.G. Chen [b], Z.Y. Liu [a,*], B.L. Xiao [a,**], Z.Y. Ma [a]

[a] Shi-changxu Innovation Center for Advanced Materials, Institute of Metal Research, Chinese Academy of Science, 72 Wenhua Road, Shenyang, 110016, China
[b] Department of Applied Science, University of Québec at Chicoutimi, Saguenay, Québec, G7H 2B1, Canada

ARTICLE INFO

Keywords:
Metal-matrix composites (MMCs)
Carbon nanotube
Fatigue
Powder processing

ABSTRACT

Heterogeneous structure consisting of brittle-zones (BZs) rich of carbon nanotubes (CNTs) and ductile-zones (DZs) free of CNTs, was an effective way to improve the strength-ductility of CNT reinforced Al (CNT/Al) composites. Two heterogeneous CNT/2009Al composites with coarse grain (CG, ~2 μm) DZs or ultra-fine grain (UFG, ~500 nm) DZs were fabricated and achieved enhanced strength-ductility. However, the heterogeneous composite with CG DZs had a lower high-cycle fatigue strength as well as fatigue strength/tensile strength ratio than the uniform composite, while the heterogeneous composite with UFG DZs exhibited the increased fatigue strength and the same level of fatigue strength/tensile strength ratio compared to the uniform composite. It was found that the improved fatigue properties for the heterogeneous composite with the UFG DZs could attribute to two reasons. Firstly, the UFG for the DZs significantly increased the strength of DZs, which effectively reduced the strain localization in the DZs. Secondly, the dislocations piling up at the grain boundaries of the BZs, as well as the stress concentration at the boundaries between the DZs and BZs were relieved due to the coordinated micro-strain for the heterogeneous structure. This provided a simple strategy for the structural design of heterogeneous composites with high fatigue strength.

1. Introduction

With the continuous upgrading of high-tech equipment in aerospace, electronics, nuclear power and other fields, the demand for metal matrix composites (MMCs) with strong structural and performance designability, excellent physical and mechanical properties is growing rapidly [1–7]. Among them, carbon nanotube (CNT) reinforced Al matrix (CNT/Al) composites have attracted great attention due to their high specific strength, high specific modulus and good machinability [8–18]. However, the CNT/Al composites have a significant drawback of low ductility, which limits their industrial application. This is mainly due to the lower dislocation storability of the fine grains, and the strong pinning effect of CNTs on dislocation gliding [19–21].

The heterogeneous structures consisting of ductile-zones (DZs) and brittle-zones (BZs) by varied distribution of reinforcements or grain sizes, have been demonstrated as a promising approach to have a better trade off of the strength-ductility in ultrafine grained (UFG) metals and composites [22–28]. Recently, some scholars studied the heterogeneous CNT/Al composites, and found that they had better strength-ductility than the uniform CNT/Al composites [29–34]. For example, Liu et al. [31] fabricated the heterogeneous CNT/Al-Cu-Mg composite by powder metallurgy method combined with subsequent hot extrusion, and reported that it achieved more than 100% elongation increase with nearly no loss of the tensile strength as compared to the uniform CNT/Al-Cu-Mg composite. The enhanced elongation was attributed to the greatly suppressed strain localization and effectively blunted micro-cracks due to the inhomogeneous structure. Meanwhile, geometrically necessary dislocations were induced between the DZs and BZs, leading to extra-strengthening beyond the rule-of-mixtures. On the basis of the toughening strategy with heterogeneous structures, Tan et al. [34] fabricated the heterogeneous CNT/Al-Cu-Mg composite with trimodal grain structure, and found that both the elongation and tensile strength of the heterogeneous composite were higher than the uniform composite. This achievement in heterogeneous CNT/Al composites further confirmed the beneficial role of tailoring grain structure in improving the strength-ductility of CNT/Al composites.

For many industrial applications, the fatigue performance is a key criterion of structural materials. Therefore, it is of great importance to

* Corresponding author.
** Corresponding author.
E-mail addresses: zyliu@imr.ac.cn (Z.Y. Liu), blxiao@imr.ac.cn (B.L. Xiao).

https://doi.org/10.1016/j.compositesb.2021.109094
Received 10 May 2021; Received in revised form 16 June 2021; Accepted 17 June 2021
Available online 22 June 2021

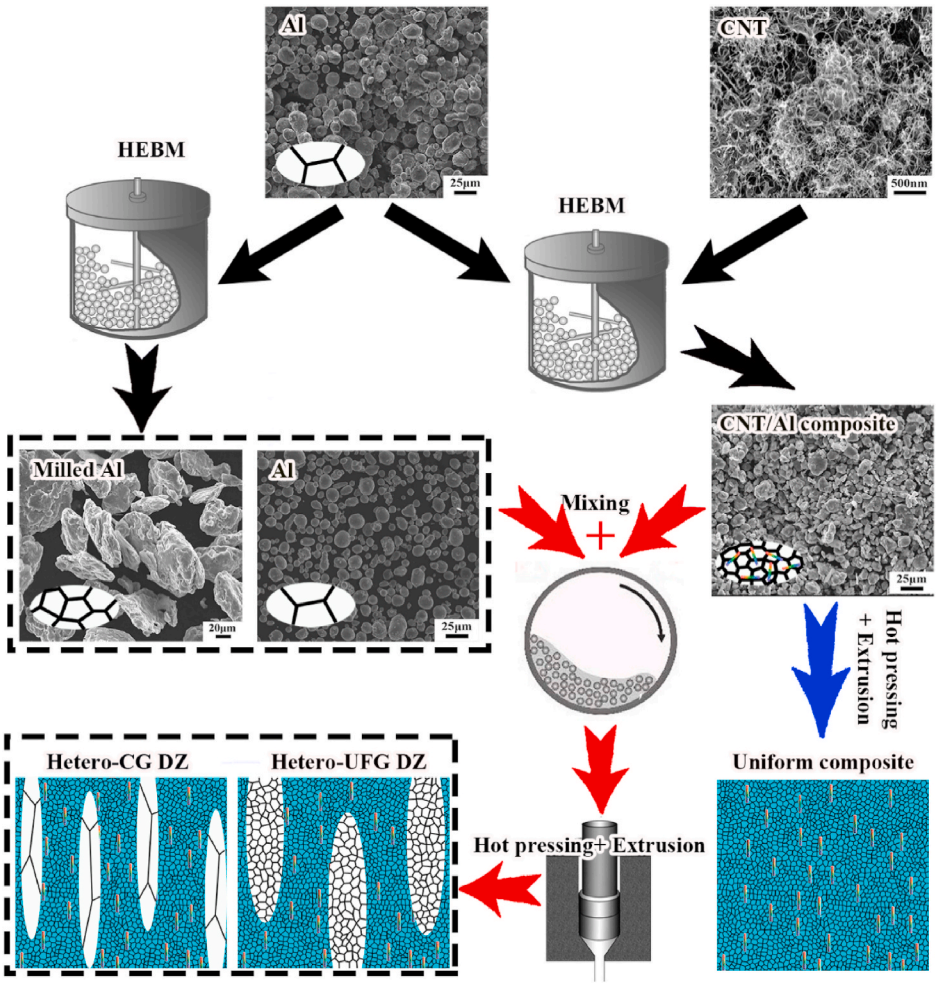

Fig. 1. Schematic of the fabrication process of CNT/2009Al composites with heterogeneous and uniform structures.

investigate the fatigue behavior. So far, the investigations of the heterogeneous materials were mainly focused on their tensile properties, investigations on the fatigue behaviors were quite rare. The fatigue behaviors of the uniform CNT/Al composites were investigated in recent years [35,36]. Shin et al. [35] found that the addition of CNTs was helpful to improve the fatigue strength, which was mainly due to that the prevailing bridging behavior of CNTs suppressed the formation of catastrophic cracks. However, for the heterogeneous CNT/Al composites, there was no related study on their fatigue behaviors.

According to the traditional view, the high-cycle fatigue (HCF) strength of the uniform materials was closely related to their static tensile strength, and the high static tensile strength usually corresponded to the high value of the fatigue strength [35,37,38]. On the other hand, the fatigue cracks preferentially nucleated in the local deformation area, which deteriorated the fatigue properties. For example, Nelson et al. [39] found that the HCF cracks of the heterogeneous Al alloys nucleated in the low-strength coarse grained (CG) zones. Liu et al. [40] found that the HCF strength of the Cu-Al alloys mainly depended on the most vulnerable area within the inhomogeneous grain structure, and had less relation on the overall static mechanical properties. Therefore, it was generally believed that the inhomogeneous microstructure might not be good for the improvement of the fatigue properties. This poses a challenge for the application of heterogeneous composites under the fatigue conditions.

In recent years, some researchers found that the gradient materials with the grain transition from the nano-size at the sample surface to the micro-size at the sample center had the excellent fatigue properties. For example, Lu et al. [41] and Zhang et al. [42] fabricated Cu and TWIP steels with gradient grain structure respectively, and found that their HCF strengths were higher than those of CG and UFG counterparts. Qian et al. [43] studied the fatigue behavior of heterogeneous nickel with different grain sizes in the DZs, and found that the HCF strength was significantly improved as the grain size in the DZs was lower than 1 μm, which was even higher than that of the uniform UFG nickel. However, the mechanism of improving fatigue performance has not been well understood. It is not clear yet whether adjusting the grain size in the DZs could improve the fatigue performance of heterogeneous CNT/Al composites.

In this study, the heterogeneous CNT/Al composites with two different grain sizes in the DZs as well as the uniform CNT/Al composite were fabricated by powder metallurgy route. The fatigue performance and cyclic lives at different stress amplitudes were tested and the microstructures were analyzed. The aim is to (a) clarify the effect of heterogeneous structure on the fatigue properties, and (b) develop heterogeneous CNT/Al composites with high fatigue strength without reducing the strength-ductility.

2. Experimental

In the present work, CNT/Al composites with heterogeneous structures were fabricated through powder metallurgy routes, as shown in Fig. 1. Atomized 2009Al (Al-4 wt.% Cu-1.5 wt% Mg) powders with approximately 10 μm diameters were used as raw metal materials. CNTs (~98% purity) fabricated by chemical vapor deposition had an outer

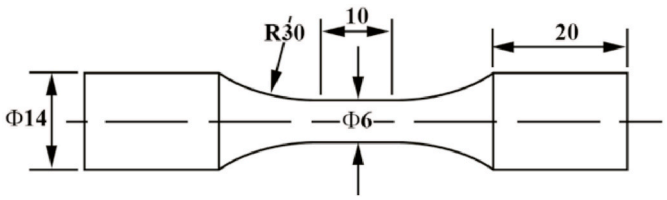

Fig. 2. The drawing of the fatigue sample (all dimensions in mm).

diameter of 10–30 nm and a length of ~5 μm. No extra pre-treatment was conducted on CNTs. 3 vol% CNTs were high energy ball milled with 10 μm as-received 2009Al powders at a rotation rate of 250 rpm with a ball to powder ratio of 15:1 for 10 h using an attritor, obtaining the milled CNT/2009Al composite powders.

In order to fabricate heterogeneous composites with different grain sizes in the DZs, two different 2009Al matrix powders, namely the as-received and the milled 2009Al powders were used, respectively. The milled 2009Al powders were obtained using high energy ball milling (HEBM) process, which was similar to that for the milled CNT/2009Al composite powders, but with the HEBM time of 4 h. 25% of these two matrix powders were respectively mixed with the ball milled CNT/2009Al composite powders using a dual axis mixer at a rotation rate of 50 rpm for 6 h, thereby obtaining two kinds of as-mixed heterogeneous composite powders.

The as-mixed composite powders were cold compacted and then vacuum hot pressed into billets under a pressure of 50 MPa at 813 K. The billets were extruded into bars at 743 K with an extrusion ratio of 16:1. The extruded bars were solution treated at 770 K for 2 h, quenched into water and naturally aged for 4 days (T4 state). For convenience, the final heterogeneous composites prepared by mixing the milled composite powders with as-received or milled 2009Al alloy powders were respectively abbreviated as Hetero-CG DZ and Hetero-UFG DZ.

For comparison, the uniform 2.25 vol% CNT/2009Al composite was also fabricated. The fabrication process was similar to that for the heterogeneous CNT/2009Al composites, but no additional 2009Al matrix powders were mixed with the milled CNT/2009Al composite powders. The uniform 2.25 vol% CNT/2009Al composite was simplified as Uniform composite. Tensile specimens with a gauge diameter of 5 mm and a length of 30 mm were machined from the extruded bars (T4 state) with the axis parallel to the extrusion direction. Tensile tests were carried out at a strain rate of 10^{-3} s^{-1} using an Instron 8862 tester. An Instron static axial clip-on extensometer with a gauge length of 25 mm was used to measure the El.

The samples with T4 state for fatigue testing were machined from the extruded bars with the axis parallel to the extrusion direction, and the dimension of the fatigue sample is shown in Fig. 2. HCF tests were performed using servo-hydraulic facility equipment (Instron 8801 tester) under the load-controlled mode at a frequency of 20 Hz and a stress ratio of $R = \sigma_{min}/\sigma_{max} = 0.1$ ($\sigma_{min}$and σ_{max} are the minimum and maximum applied stresses, respectively) at room temperature. 4-5 stress amplitudes were chosen for the fatigue testing, and two samples were chosen for fatigue testing under each stress amplitude. The microstructures were characterized by optical microscopy (OM; Zeiss Axiovert 200 MAT), scanning electron microscopy (SEM; JSM-6480LV) and transmission electron microscopy (TEM; JEM-2100). The TEM samples for observing the initial microstructure were cut from the extruded bars with the foil plane parallel to the extrusion direction, and the TEM samples for observing the microstructure after fatigue were cut from the fatigue samples near the fracture surface, with the foil plane vertical to the loading direction. All the thin foils for TEM were ground to a thickness of 60 μm, punched to disks with a diameter of 3 mm, then dimpled to a minimum thickness of 20 μm and finally ion-beam thinned by a Gatan Model 691 ion milling system.

3. Results and discussion

3.1. Initial microstructure

Fig. 3 shows the OM images of the two kinds of heterogeneous CNT/2009Al composites. It can be seen that the bright zones aligned along the extrusion direction were embedded in the dark zones. According to our previous investigations [30–32], the bright zones were the DZs originating from the additional matrix powders, and the dark zones were the BZs originating from the milled CNT/Al composite powders. The DZ bands for the Hetero-CG DZ were slightly thinner (Fig. 3(a)) than those of the Hetero-UFG DZ (Fig. 3(b)). According to the dimension statistical analysis of at least 100 DZ bands for each composite, the average DZ band widths of the Hetero-CG DZ and Hetero-UFG DZ were measured to be 2.6 and 6.6 μm, respectively. The difference in the DZ bands between the Hetero-UFG DZ and Hetero-CG DZ was mainly caused by the different dimensions of the additional mixed 2009Al powders. For the Hetero-UFG DZ, the added 2009Al powders underwent 4 h HEBM process. The cold-welding of the powders during the HEBM process led to the increase of the powder dimension. As a result, the DZ width of the Hetero-UFG DZ was larger than that of the Hetero-CG DZ.

Fig. 4 shows the TEM images of grain morphologies and CNT distribution in different CNT/2009Al composites. It can be seen that the grains in the Uniform composite were very small, with the average grain size of ~200 nm (Fig. 4(a)). For heterogeneous composites, their grain morphologies in the BZs of the two heterogeneous composites were similar with that of the Uniform composite. CNTs with average length of ~100 nm (marked by black arrows) were uniformly distributed in the BZs (Fig. 4(d)). High resolution TEM image indicates that the interface between CNT and Al matrix was well bonded, and the structure integrity of CNTs maintained well (Fig. 4(e)).

However, the grain morphologies in the DZs of these two heterogeneous composites were quite different. For the Hetero-CG DZ, the grain width in the DZs was ~2 μm, and the grain length was larger than 5 μm (Fig. 4(b)). For the Hetero-UFG DZ, the grains in the DZs were

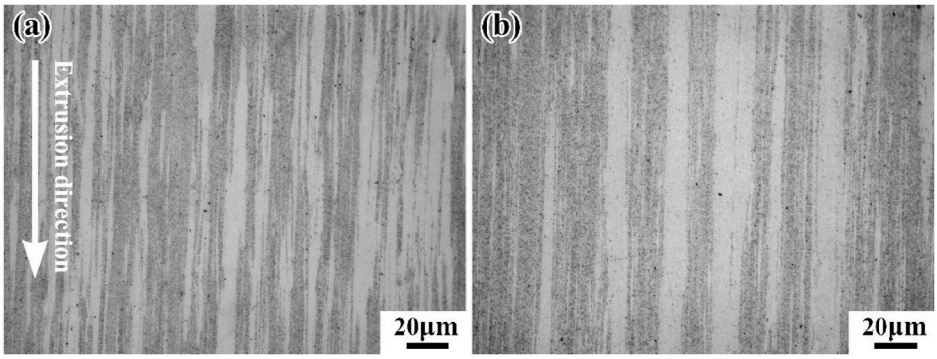

Fig. 3. OM images of BZ and DZ morphologies in the heterogeneous composites: (a) Hetero-CG DZ and (b) Hetero-UFG DZ.

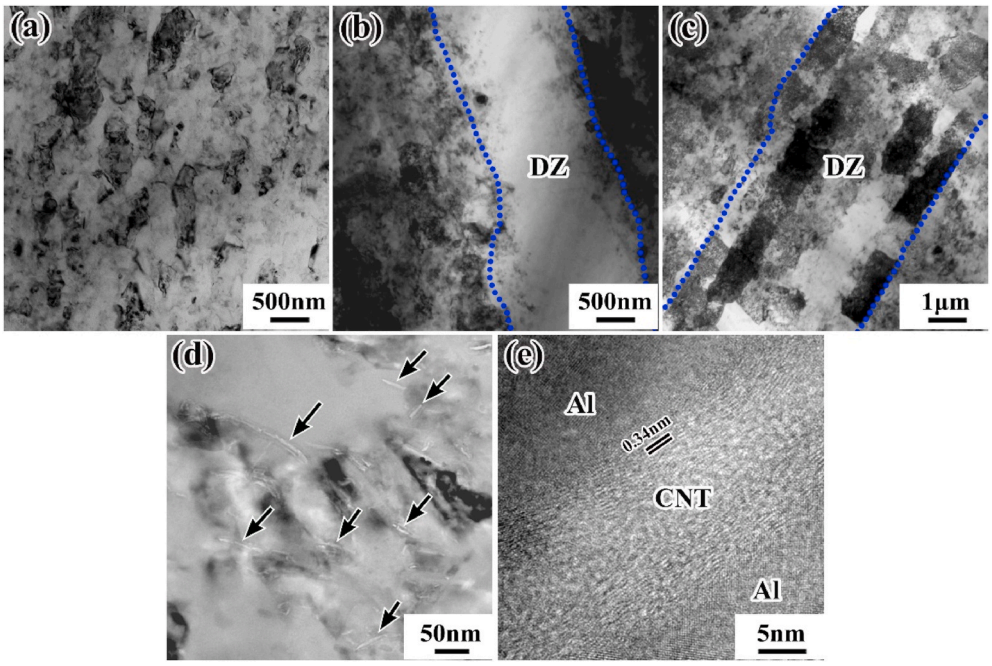

Fig. 4. TEM images of (a) Uniform composite, (b) Hetero-CG DZ, (c) Hetero-UFG DZ (Blue lines in (b) and (c) are the boundaries between the DZs and BZs), (d) CNT distribution (indicated by black arrows) and (e) High resolution TEM image showing CNT-Al interface in the BZs. (For interpretation of the references to colour in this figure legend, the reader is referred to the Web version of this article.)

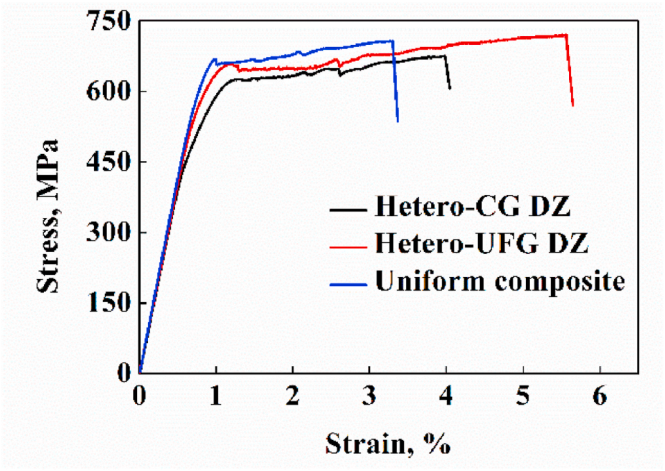

Fig. 5. Tensile properties of the uniform and heterogeneous composites.

Table 1
Mechanical and fatigue properties of the three CNT/2009Al composites with different structures.

Sample	Tensile properties				Fatigue properties	
	YS (MPa)	UTS (MPa)	El (%)	UTS × El (MJ/m^3)	σ_{FS} (MPa)	m
Uniform composite	671 ± 5	707 ± 5	2.5 ± 0.2	16.7	450	0.64
Hetero-CG DZ	574 ± 5	680 ± 8	3.8 ± 0.5	25.8	420	0.62
Hetero-UFG DZ	620 ± 7	720 ± 6	4.7 ± 0.5	33.8	460	0.64

significantly refined, with the average grain width of ~500 nm and the grain length of ~2 μm (Fig. 4(c)). The grain refinement in the DZs for the Hetero-UFG DZ was caused by the severe plastic deformation during the HEBM process.

3.2. Tensile and high-cycle fatigue properties

Tensile stress-strain curves for the Uniform composite, Hetero-CG DZ and Hetero-UFG DZ are shown in Fig. 5. The Uniform composite had a high yield strength (YS) of 671 MPa and a high ultimate tensile strength (UTS) of 707 MPa, but the elongation (El) was as low as 2.5%. Compared with the Uniform composite, the both heterogeneous composites exhibited a much higher strength ductility product (UTS × El), which demonstrates an enhanced strength-ductility of the heterogeneous structure. All the mechanical and fatigue properties are listed in Table 1. By comparing the tensile properties of two heterogeneous composites, it can be seen that all the tensile properties (including the YS, UTS and El) of the Hetero-UFG DZ were higher than that of the Hetero-CG DZ, which demonstrates that the strength-ductility of the Hetero-UFG DZ was better than that of the Hetero-CG DZ.

The stress amplitudes versus the numbers of cycles-to-failure (N_f) are shown in Fig. 6(a), and the arrows indicate that the specimens did not fail. Similar to that for most of other materials, the fatigue life of the composites decreased as the applied stress increased. At a certain N_f, the stress amplitude of the Hetero-CG DZ, Uniform composite and Hetero-UFG DZ increased in turn, which indicates that the Hetero-UFG DZ exhibited the best fatigue performance. As the N_f reaches to 10^6–10^7 cycles, the corresponding maximum stress can be determined as fatigue strength σ_{FS} [44]. In general, high ultimate tensile strength σ_{UTS} usually leads to a high fatigue strength [45]. The ratio of σ_{FS} to σ_{UTS} could be given by Eq. (1) [35]:

$$m = \sigma_{FS}/\sigma_{UTS} \quad (1)$$

The value of m, a parameter determined from the experimental data for many metallic materials such as iron, copper, and Al alloys, has been well established. According to a large number of fatigue data for these materials, m are estimated to be 0.4–0.6 for steels and Al alloys [44,46].

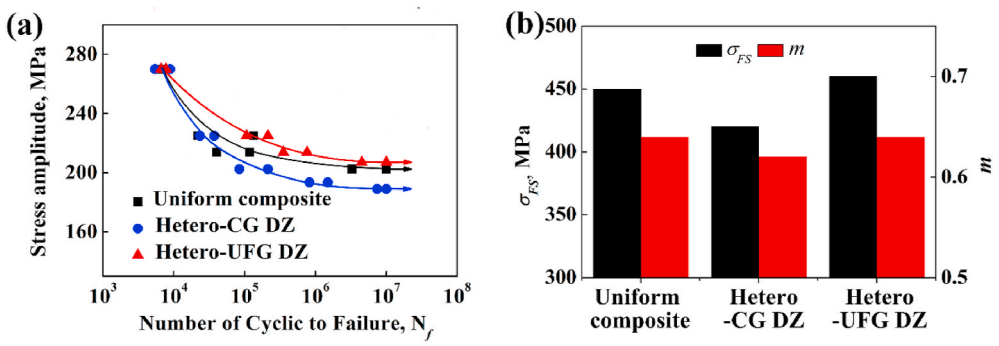

Fig. 6. (a) Stress amplitude versus the number of cycles to failure curve, (b) σ_{FS} and m for different composites.

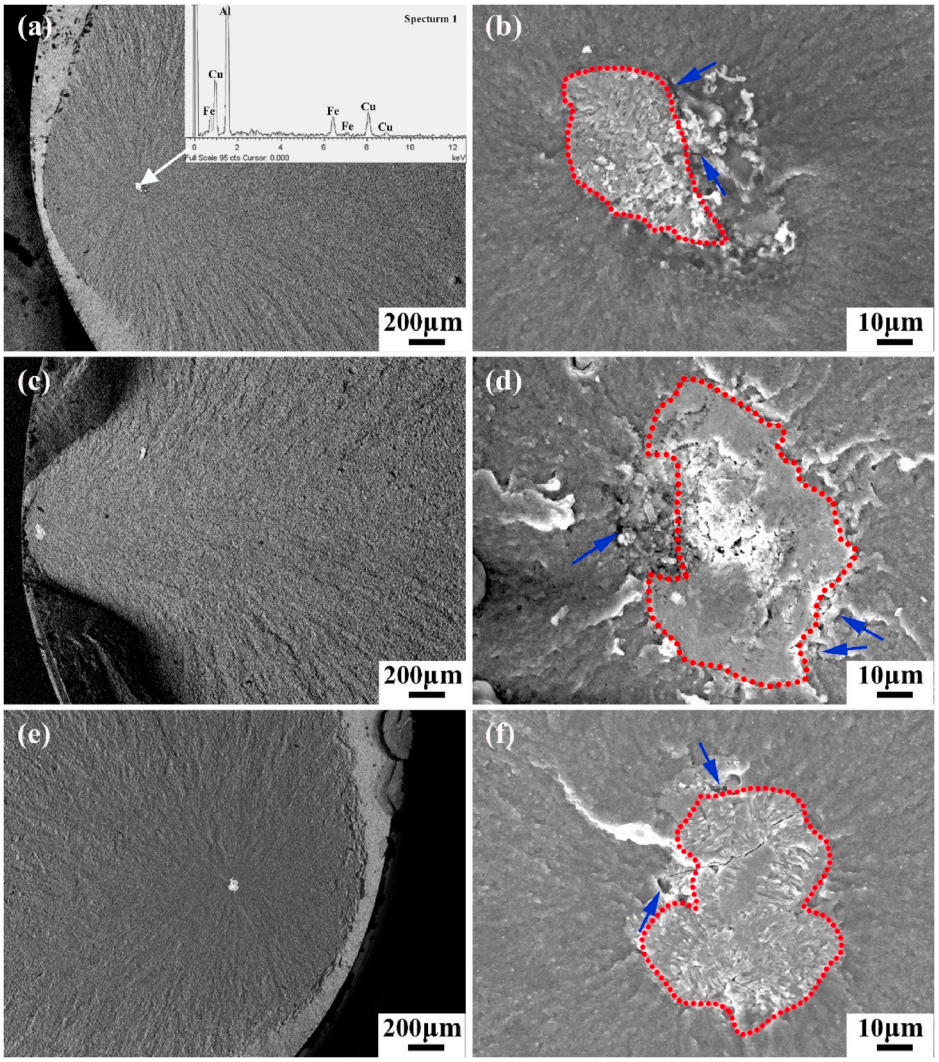

Fig. 7. SEM images showing the fatigue crack initiation sites on the fracture surfaces of (a)(b) Uniform composite (stress amplitude of 203 MPa, 3.3×10^6 cycles to failure), (c)(d) Hetero-CG DZ (stress amplitude of 189 MPa, 7.4×10^6 cycles to failure), (e)(f) Hetero-UFG DZ (stress amplitude of 207 MPa, 4.5×10^6 cycles to failure) (Red circles indicate the Fe-rich inclusions and blue arrows indicate the voids). (For interpretation of the references to colour in this figure legend, the reader is referred to the Web version of this article.)

As shown in Fig. 6(b) and Table 1, all the composites had a high m, which was higher than 0.6. However, the m of Hetero-CG DZ was a little lower than that of the other two composites.

The high fatigue strength and high m value of the uniform CNT/Al composites were reported by Shin et al. [35]. They found that the more CNT content led to the higher fatigue strength and m value. The enhanced fatigue performance was mainly attributed to that the prevailing bridging behavior of CNTs could inhibit the propagation of cracks. In the present work, all the three composites had the same CNT content of 2.25 vol%, expecting the similar influence of CNTs on high fatigue strength and m value. Therefore, the different fatigue strengths and m values should be related to the CNT distribution and heterogeneous structure, which will be discussed in the next section.

3.3. Fractograph analysis

Fig. 7 shows the typical crack initiation sites for different composites. It can be found that all the three composites had the similar crack nucleation feature that the radial striations converged at the inclusion near the surface of the specimens (Fig. 7(a)(c)(e)). The inclusion size was

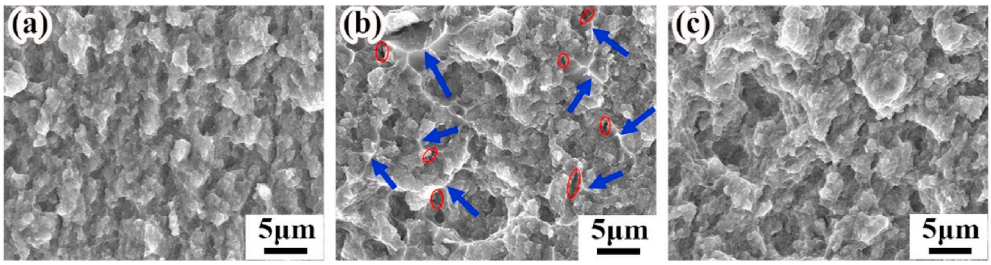

Fig. 8. Fracture morphologies at the center of the samples: (a) Uniform composite (stress amplitude of 203 MPa, 3.3×10^6 cycles to failure), (b) Hetero-CG DZ (stress amplitude of 189 MPa, 7.4×10^6 cycles to failure), (c) Hetero-UFG DZ (stress amplitude of 207 MPa, 4.5×10^6 cycles to failure) (Red circles indicate the micro-cracks and blue arrows indicate the tear ridges). (For interpretation of the references to colour in this figure legend, the reader is referred to the Web version of this article.)

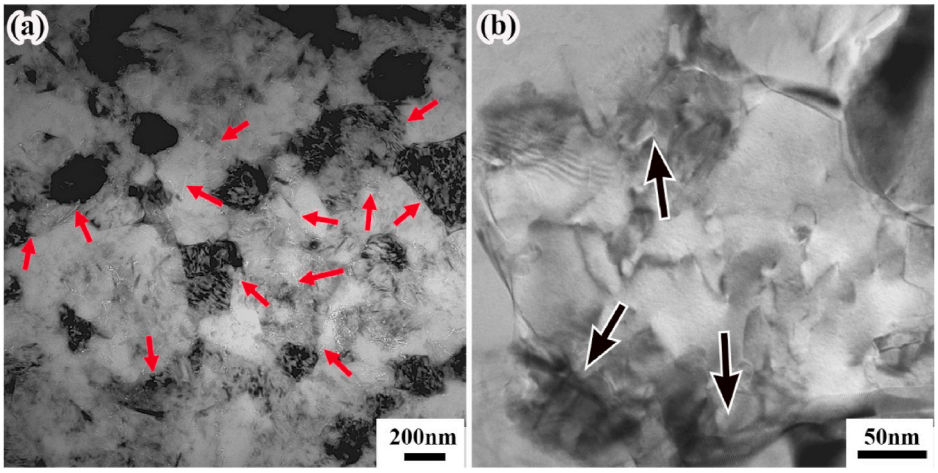

Fig. 9. TEM images of the Uniform composite after fatigue test (stress amplitude of 203 MPa, 3.3×10^6 cycles to failure): (a) grain and CNT distribution (CNTs indicated by red arrows), (b) dislocation morphology (Black arrows indicate the dislocations piling up at the GBs). (For interpretation of the references to colour in this figure legend, the reader is referred to the Web version of this article.)

approximately 30–50 μm, and some voids or micro-cracks (marked by arrows) were observed at the interfaces between the inclusion and matrix (Fig. 7(b)(d)(f)). All the inclusions were determined to be rich in Fe by SEM-energy dispersive spectrometry. That is, fatigue crack nucleation of all the three composites took place at Fe-rich inclusions near the specimen surface.

Since CNTs were dispersed into the matrix powders by the HEBM method, after a long period of severe collision, the steel balls would inevitably introduce some impurities such as steel filings into the powders. As the powders were hot-consolidated at elevated temperature, Fe-rich inclusions formed [47]. The Fe-rich inclusions as the fatigue crack initiation were also widely reported in other Al alloys and Al matrix composites [48,49].

Fig. 8 shows the fractograph away from the specimen surfaces. No obvious fatigue striations were observed in all the three specimens, which indicates rapid fracture occurred after crack initiation. For the Uniform composite, the dimples were small (Fig. 8(a)), while the dimples were a little larger for the heterogeneous composites (Fig. 8(b)(c)). Furthermore, many tear ridges (marked by blue arrows) were found within the Hetero-CG DZ. No CNTs could be found in the tear ridges, referring that the tear ridges were formed by the DZs. Some micro-cracks (marked by red circles) distributed at the edges of the tear ridges in the Hetero-CG DZ as shown in Fig. 8(b), indicating that there were stress concentrations at the boundaries between the DZs and BZs. The occurrence of stress concentration should be responsible for the low fatigue strength and *m* of the Hetero-CG DZ.

3.4. Damage mechanism

Fig. 9 displays the TEM images of the Uniform composite after fatigue test. It can be seen that the grain size still retained as small as about 200 nm, while CNTs were uniformly distributed within the matrix (marked by red arrows in Fig. 9(a)). The phenomenon of stable grain size after fatigue test for the UFG composites was quite different from that for the UFG Al alloys [38,50]. Goswami et al. [50] reported that UFG Al would coarsen after fatigue test, because the adjacent fine grains tended to align under cyclic stress. For the CNT/Al composites, a large number of CNTs were embedded in the matrix, which had a strong pinning effect on grain boundaries (GBs) and would prohibit the grain growth during the fatigue testing, leading to the stable grain size. Meanwhile, according to the Hall-Petch relationship, the smaller grain size led to the higher strength [19]. Therefore, the stable and small grain size would be responsible for the high fatigue strength and *m* of the Uniform composite.

The magnified image of the UFG indicates that some entangled dislocations were formed within the grains, and dislocations piled up at the GBs (marked by black arrows in Fig. 9(b)). It is well known that the boundaries as a barrier can inhibit the movement of dislocations, and the piled-up dislocations will further develop into micro-crack defects under cyclic loading [51]. Therefore, the failure mode of the Uniform composite could be inferred that the dislocation piling up at the GBs promoted the crack nucleation and then the cracks propagated to cause the material failure.

Fig. 10 shows the TEM images of the heterogeneous composite specimens after fatigue test. For the Hetero-CG DZ, a small number of dislocations can be observed within the grains of BZs, and no obvious

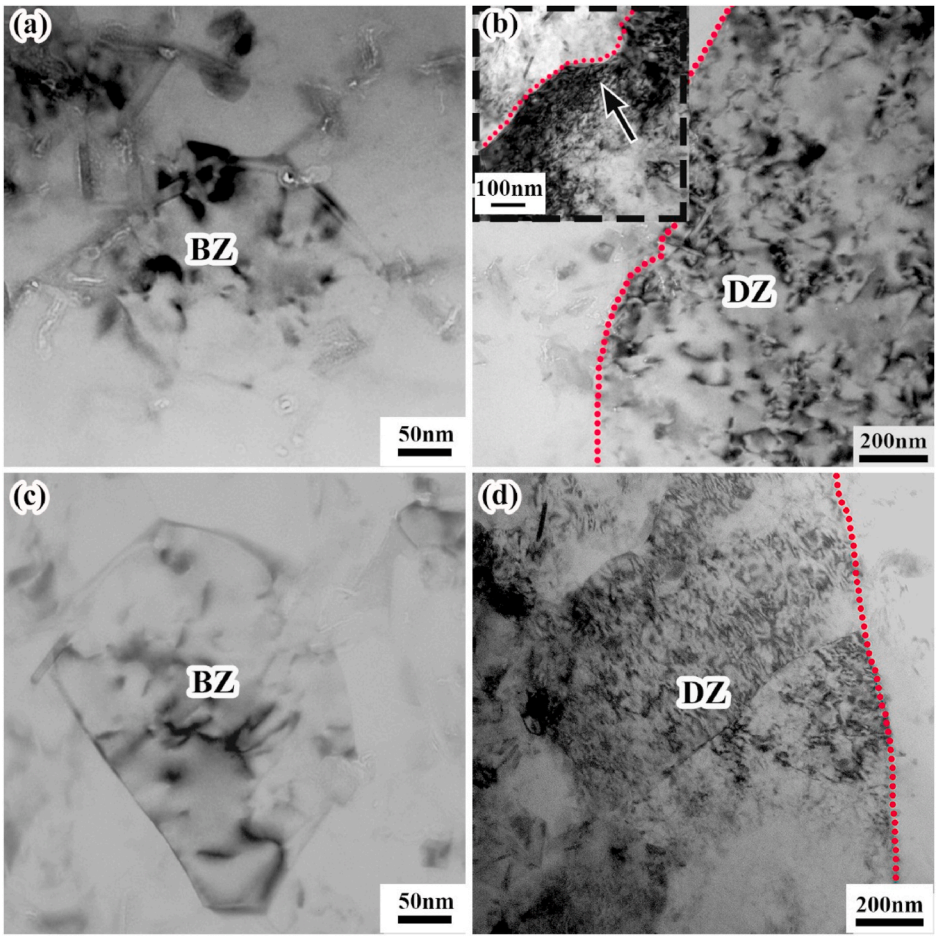

Fig. 10. TEM images of (a)(b) the Hetero-CG DZ after fatigue test (stress amplitude of 189 MPa, 7.4 × 10^6 cycles to failure), (c)(d) the Hetero-UFG DZ after fatigue test (stress amplitude of 207 MPa, 4.5 × 10^6 cycles to failure) (Red lines are the boundaries between the DZs and BZs). (For interpretation of the references to colour in this figure legend, the reader is referred to the Web version of this article.)

piled-up dislocations were observed at the GBs (Fig. 10(a)). Compared with that of the Uniform composite, the reduced dislocation density in the BZs of the Hetero-CG DZ could attribute to the more deformation in the low-strength DZs. This could be reflected in the TEM image of DZs in the Hetero-CG DZ (Fig. 10(b)). A large number of dislocations could be observed in the DZs, indicating the preferential deformation in the DZs. Nelso et al. [39] investigated the HCF behavior of the heterogeneous Al alloys. They found that the DZs with lower strength preferentially deformed, and the fatigue life of the heterogeneous Al alloys was lower than that of the uniform counterpart. The low fatigue strength of the Hetero-CG DZ in the present study agreed well with the Nelso's investigation.

In addition to reducing the overall strength of the material by mixing the low-strength CG DZs, the stress concentration at the boundaries between the DZs and BZs that would accelerate the fatigue damage was also an important reason to decrease the fatigue strength. As shown by the black arrow inside of Fig. 10(b), a large number of dislocations were accumulated at the boundaries between the DZs and BZs, indicating the serious stress concentration at the boundaries between the DZs and BZs. This was in accordance with the fractograph as shown in Fig. 8(b), where there were many cracks at the edge of the DZs. Because the significant stress concentration would promote crack nucleation, the m would also be low. On the whole, both the addition of low-strength CG DZs and the stress concentration at the boundaries between the DZs and BZs would decrease the σ_{FS} of the Hetero-CG DZ.

For the Hetero-UFG DZ, a few dislocations could be observed within the grains in the BZs, and no obvious piled-up dislocations were observed at the GBs (Fig. 10(c)). However, the dislocation distribution in the DZs for the Hetero-UFG DZ was quite different from that for the Hetero-CG DZ, the dislocations only occurred at some parts of the DZs (Fig. 10(d)). This was because that the DZs contained many grains in the Hetero-UFG DZ, dislocations tended to move within the crystal plane that facilitates slipping. Due to the different crystal orientations between adjacent grains in the DZs, the continuous movement of dislocations would be interrupted at the GBs. The deformation concentration area in the DZs was divided into multiple smaller-sized units by the inner GBs, so the deformation concentration in the DZs would be weakened. Further, the grains of the DZs were refined by HEBM, which reduced the grain size difference between the DZs and BZs, and further relaxed the stress concentration at the boundaries between the DZs and BZs. The grain refinement in the DZs led to the increase of the strength and the decrease of the stress concentration, resulting in the enhanced fatigue properties (including the σ_{FS} and m) of the Hetero-UFG DZ, as compared with those of the Hetero-CG DZ.

It should be mentioned that, the m of the Hetero-UFG DZ was the same as that of the Uniform composite and the σ_{FS} of the Hetero-UFG DZ was even slightly higher than that of the Uniform composite. The high m of the Hetero-UFG DZ was believed to result from the following two reasons. On one hand, the grain size difference between the DZs and BZs was very small, so the stress concentration at the boundaries between the DZs and BZs could be easily relaxed. On the other hand, the dislocations piling up at the boundaries of the BZs were relieved due to the coordinated micro-strain for the heterogeneous structure, which extended the life time of the BZs. Finally, because the Hetero-UFG DZ

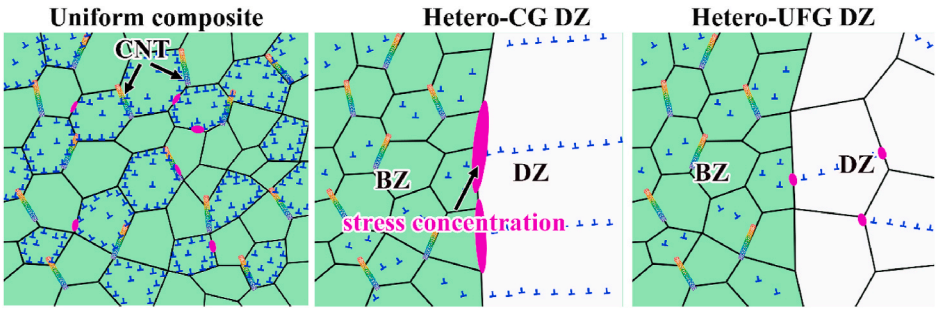

Fig. 11. Schematic illustration of deformation behavior and damage mechanism of the three CNT/2009Al composites (Uniform composite, Hetero-CG DZ and Hetero-UFG DZ).

had the higher UTS and the same *m* as the Uniform composite, the σ_{FS} of the Hetero-UFG DZ would be higher than that of the Uniform composite.

The damage mechanism of the uniform and heterogeneous CNT/2009Al composites under the cyclic loading can be schematically summarized in Fig. 11. For the Uniform composite, the GBs were pinned by CNTs and no obvious grain coarsening could be observed. Under the fatigue stress, dislocations slipped inside the grains and piled up at the GBs. As the cycle number increased, the dislocations piling up at the GBs increased, and eventually cracks nucleated at the GBs, resulting in fatigue fracture.

For the Hetero-CG DZ, due to the introduction of the CGs in the DZs with lower strength, the cyclic deformation preferred to develop in the DZs, so the dislocation distribution in the DZs was much denser than that in the BZs. Because the deformation portion in the BZs was reduced, the dislocation accumulation at the GBs in the BZs became weaker. However, due to the large deformation mismatch between the DZs and BZs, the stress concentration at the boundaries between the DZs and BZs was severe, and microcracks were also easy to nucleate at the boundaries between the DZs and BZs. With the addition of low-strength DZs and significant stress concentration at the boundaries between the DZs and BZs, the fatigue properties of the Hetero-CG DZ were the weakest among the three composites.

For the Hetero-UFG DZ, the grain size in the DZs was much smaller as compared with that for the Hetero-CG DZ, which resulted in a higher strength of the DZs. Because the grain size difference between the BZs and DZs was quite small, the stress concentration at the boundaries between the DZs and BZs in the Hetero-UFG DZ was much lower than that in the Hetero-CG DZ. Furthermore, the strain localization in the BZs was decreased due to the heterogeneous structure. As a result, the σ_{FS} of the Hetero-UFG DZ was the highest among the three composites and the *m* of the Hetero-UFG DZ was as high as that of the Uniform composite.

4. Conclusions

In this study, the uniform and two kinds of heterogeneous CNT/2009Al composites with different grain sizes in the DZs were fabricated by powder metallurgy routes. The high cycle fatigue tests with the stress ratio of 0.1 and frequency of 20 Hz were carried out, and the microstructures before and after fatigue test were analyzed. The following conclusions can be drawn:

(1) All the three CNT/2009Al composites, including the uniform composite, the heterogeneous composite with coarse grain ductile-zones and the heterogeneous composite with ultrafine grain ductile-zones exhibited high fatigue strength/tensile strength ratio (*m*), with *m* values of 0.64, 0.62 and 0.64, respectively.

(2) For the heterogeneous composites with coarse grained ductile-zones, the fatigue strength was lower than that of the uniform composite, due to the introduction of low-strength coarse grain ductile-zones and significant stress concentration at the boundaries between the ductile-zones and brittle-zones.

(3) The ultra-fine grain of the ductile-zones could effectively increase the strength of the ductile-zones. The ultra-fine grain of the ductile-zones also reduced the grain difference between brittle-zones and ductile-zones, which relaxed the stress concentration at the boundaries between the ductile-zones and brittle-zones. Further, the heterogeneous structure could reduce the dislocations piling up at grain boundaries in the brittle-zones. As a result, the fatigue strength of the heterogeneous composite with the ultra-fine grain ductile-zones was higher than that of the uniform composite while maintaining its good strength-ductility.

Author statement

All authors contribute substantially to the paper. K. Ma (first author) carried out the data collection, data analysis and manuscript writing; X. N. Li fabricated the composites and tested the tensile properties; K. Liu, X.G. Chen helped to revise the manuscript; Z.Y. Liu designed the experiment and revised the manuscript; B.L. Xiao participated in the design of the experiment and analysis of the experimental data; Z.Y. Ma revised the manuscript and provided the funding. All authors read and approved the final manuscript.

Declaration of competing interest

The authors declare that they have no known competing financial interests or personal relationships that could have appeared to influence the work reported in this paper.

Acknowledgements

This work was supported by: (a) Key R&D Program of China under grant (No. 2017YFB0703104); (b) Key Research Program of Frontier Sciences, CAS (NO. QYZDJ-SSW-JSC015); (c) National Natural Science Foundation of China (No. 51871215, No. 51931009, No.51871214); (d) the Youth Innovation Promotion Association CAS (2020197). K. Ma would like to acknowledge the support from China Scholarship Council.

References

[1] Xiao BL, Huang ZY, Ma K, Zhang XX, Ma ZY. Research on hot deformation behaviors of discontinuously reinforced aluminum composites. Acta Metall Sin 2019;55(1):59–72.

[2] Ma K, Zhang XX, Wang D, Wang QZ, Liu ZY, Xiao BL, et al. Optimization and simulation of deformation parameters of SiC/2009Al composites. Acta Metall Sin 2019;55(10):1329–37.

[3] Liu J, Fan G, Tan Z, Guo Q, Su Y, Li Z, et al. Mechanical properties and failure mechanisms at high temperature in carbon nanotube reinforced copper matrix nanolaminated composite. Composites Part A 2019;116:54–61.

[4] Zan YN, Zhou YT, Zhao H, Liu ZY, Wang QZ, Wang D, et al. Enhancing high-temperature strength of (B_4C+Al_2O_3)/Al designed for neutron absorbing materials by constructing lamellar structure. Composites Part B 2020;183:107674.

[5] Liu ZY, Wang LH, Zan YN, Wang WG, Xiao BL, Wang D, et al. Enhancing strengthening efficiency of graphene nano-sheets in aluminum matrix composite by improving interface bonding. Composites Part B 2020;199:108268.
[6] Zhu SZ, Wang D, Xiao BL, Ma ZY. Suppressed negative effects of natural aging by pre-aging in SiCp/6092Al composites. Composites Part B 2021;212:108730.
[7] Zhang JF, Zhang XX, Andrä H, Wang QZ, Xiao BL, Ma ZY. A fast numerical method of introducing the strengthening effect of residual stress and strain to tensile behavior of metal matrix composites. J Mater Sci Technol 2021;87:167–75.
[8] Zhang X, Zhao N, He C. The superior mechanical and physical properties of nanocarbon reinforced bulk composites achieved by architecture design - a review. Prog Mater Sci 2020;113:100672.
[9] Chen B, Kondoh K, Li J, Qian M. Extraordinary reinforcing effect of carbon nanotubes in aluminium matrix composites assisted by in-situ alumina nanoparticles. Composites Part B 2020;183:107691.
[10] Liu ZY, Xiao BL, Wang WG, Ma ZY. Analysis of carbon nanotube shortening and composite strengthening in carbon nanotube/aluminum composites fabricated by multi-pass friction stir processing. Carbon 2014;69:264–74.
[11] Liu ZY, Xiao BL, Wang WG, Ma ZY. Singly dispersed carbon nanotube/aluminum composites fabricated by powder metallurgy combined with friction stir processing. Carbon 2012;50(5):1843–52.
[12] Liu ZY, Xiao BL, Wang WG, Ma ZY. Developing high-performance aluminum matrix composites with directionally aligned carbon nanotubes by combining friction stir processing and subsequent rolling. Carbon 2013;62:35–42.
[13] Liu ZY, Xiao BL, Wang WG, Ma ZY. Modelling of carbon nanotube dispersion and strengthening mechanisms in Al matrix composites prepared by high energy ball milling-powder metallurgy method. Composites Part A 2017;94:189–98.
[14] Jiang L, Li Z, Fan G, Cao L, Zhang D. The use of flake powder metallurgy to produce carbon nanotube (CNT)/aluminum composites with a homogenous CNT distribution. Carbon 2012;50(5):1993–8.
[15] Tjong SC. Recent progress in the development and properties of novel metal matrix nanocomposites reinforced with carbon nanotubes and graphene nanosheets. Mater Sci Eng R 2013;74(10):281–350.
[16] Zhang XX, Zhang JF, Liu ZY, Gan WM, Hofmann M, Andrä H, et al. Microscopic stresses in carbon nanotube reinforced aluminum matrix composites determined by in-situ neutron diffraction. J Mater Sci Technol 2020;54:58–68.
[17] Bi S, Liu ZY, Yu BH, Ma GN, Wu LH, Xiao BL, et al. Superplastic deformation behavior of carbon nanotube reinforced 7055 Al alloy composites. Mater Sci Eng, A 2020;797:140263.
[18] Bi S, Xiao BL, Ji ZH, Liu BS, Liu ZY, Ma ZY. Dispersion and damage of carbon nanotubes in carbon nanotube/7055Al composites during high-energy ball milling process. Acta Metall Sin (Eng Lett). 2021;34(2):196–204.
[19] Dong S, Zhou J, Hui D, Wang Y, Zhang S. Size dependent strengthening mechanisms in carbon nanotube reinforced metal matrix composites. Composites Part A 2015;68:356–64.
[20] Bi S, Liu ZY, Xiao BL, Zan YN, Wang D, Wang QZ, et al. Enhancing strength-ductility synergy of carbon nanotube/7055Al composite via a texture design by hot-rolling. Mater Sci Eng, A 2021;806:140830.
[21] Ma K, Liu Z, Zhang X, Xiao B, Ma Z. Fabrication of high strength carbon nanotube/7055Al composite by powder metallurgy combined with subsequent hot extrusion. Sci China Technol Sci 2021;64:1081–91.
[22] Wei H, Li ZQ, Xiong DB, Tan ZQ, Fan GL, Qin Z, et al. Towards strong and stiff carbon nanotube-reinforced high-strength aluminum alloy composites through a microlaminated architecture design. Scripta Mater 2014;75:30–3.
[23] Salama EI, Abbas A, Esawi AMK. Preparation and properties of dual-matrix carbon nanotube-reinforced aluminum composites. Composites Part A 2017;99:84–93.
[24] Ma X, Huang C, Moering J, Ruppert M, Hoeppel HW, Goeken M, et al. Mechanical properties of copper/bronze laminates: role of interfaces. Acta Mater 2016;116:43–52.
[25] Zha M, Zhang HM, Yu ZY, Zhang XH, Meng XT, Wang HY, et al. Bimodal microstructure A feasible strategy for high-strength and ductile metallic materials. J Mater Sci Technol 2018;34(2):257–64.
[26] Zhang J, Hao S, Jiang D, Huan Y, Cui L, Liu Y, et al. In situ synchrotron high-energy X-ray diffraction study of microscopic deformation behavior of a hard-soft dual phase composite containing phase transforming matrix. Acta Mater 2017;130:297–309.
[27] Wu H, Fan G, Huang M, Geng L, Cui X, Chen R, et al. Fracture behavior and strain evolution of laminated composites. Compos Struct 2017;163:123–8.
[28] Jiang L, Yang H, Yee JK, Mo X, Topping T, Lavernia EJ, et al. Toughening of aluminum matrix nanocomposites via spatial arrays of boron carbide spherical nanoparticles. Acta Mater 2016;103:128–40.
[29] Fu X, Yu Z, Tan Z, Fan G, Li P, Wang M, et al. Enhanced strain hardening by bimodal grain structure in carbon nanotube reinforced Al–Mg composites. Mater Sci Eng, A 2021;803:140726.
[30] Ma K, Liu ZY, Liu BS, Xiao BL, Ma ZY. Improving ductility of bimodal carbon nanotube/2009Al composites by optimizing coarse grain microstructure via hot extrusion. Composites Part A 2021;140:106198.
[31] Liu ZY, Ma K, Fan GH, Zhao K, Zhang JF, Xiao BL, et al. Enhancement of the strength-ductility relationship for carbon nanotube/Al–Cu–Mg nanocomposites by material parameter optimisation. Carbon 2020;157:602–13.
[32] Ma K, Liu ZY, Bi S, Zhang XX, Xiao BL, Ma ZY. Microstructure evolution and hot deformation behavior of carbon nanotube reinforced 2009Al composite with bimodal grain structure. J Mater Sci Technol 2021;70:73–82.
[33] Ma K, Liu ZY, Liu K, Chen XG, Xiao BL, Ma ZY. Structure optimization for improving the strength and ductility of heterogeneous carbon nanotube/Al–Cu–Mg composites. Carbon 2021;178:190–201.
[34] Fu X, Tan Z, Min X, Li Z, Yue Z, Fan G, et al. Trimodal grain structure enables high-strength CNT/Al-Cu-Mg composites higher ductility by powder assembly & alloying. Mater Res Lett 2021;9(1):50–7.
[35] Shin SE, Bae DH. Fatigue behavior of Al2024 alloy-matrix nanocomposites reinforced with multi-walled carbon nanotubes. Composites Part B 2018;134:61–8.
[36] Liao JZ, Tan MJ, Bayraktar E. Tension-tension fatigue behaviour of carbon nanotube reinforced aluminium composites. Mater Sci Forum 2013;765:563–7.
[37] Shukla S, Komarasamy M, Mishra RS. Grain size dependence of fatigue properties of friction stir processed ultrafine-grained Al-5024 alloy. Int J Fatig 2018;109:1–9.
[38] Yogesha KK, Joshi A, Jayaganthan R. Fatigue behavior of ultrafine-grained 5052 Al alloy processed through different rolling methods. J Mater Eng Perform 2017;26(6):2826–36.
[39] Nelson S, Ladani L, Topping T, Lavernia E. Fatigue and monotonic loading crack nucleation and propagation in bimodal grain size aluminum alloy. Acta Mater 2011;59(9):3550–70.
[40] Liu R, Tian YZ, Zhang ZJ, Zhang P, Zhang ZF. Fatigue strength plateau induced by microstructure inhomogeneity. Mater Sci Eng, A 2017;702:259–64.
[41] Long J, Pan Q, Tao N, Dao M, Suresh S, Lu L. Improved fatigue resistance of gradient nanograined Cu. Acta Mater 2019;166:56–66.
[42] Shao C, Zhang P, Wang X, Wang Q, Zhang Z. High-cycle fatigue behavior of TWIP steel with graded grains: breaking the rule of mixture. Mater Res Lett 2019;7(1):26–32.
[43] Qian T, Karaman I, Marx M. Mechanical properties of nanocrystalline and ultrafine-grained nickel with bimodal microstructure. Adv Eng Mater 2014;16(11):1323–39.
[44] Lee YL, Pan J, Hathaway R, Barkey M. Fatigue testing and analysis: theory and practice. Elsevier: Butterworth-Heinemann; 2005.
[45] Fatemi A, Plaseied A, Khosrovaneh AK, Tanner D. Application of bi-linear log–log S–N model to strain-controlled fatigue data of aluminum alloys and its effect on life predictions. Int J Fatig 2005;27(9):1040–50.
[46] Pang J, Li S, Wang Z, Zhang Z. Relations between fatigue strength and other mechanical properties of metallic materials. Fatig Fract Eng Mater Struct 2014;37(9):958–76.
[47] Wang AQ, Liu P, Xie JP, Wang WY, Li JW, Sun HL, et al. Interface characterization, precipitate evolution, and quantitative modeling of the microstructure/strength relationship in SiCp/2024Al composite. Compos Interfac 2015;22(9):847–66.
[48] Xue Y, El Kadiri H, Horstemeyer MF, Jordon JB, Weiland H. Micromechanisms of multistage fatigue crack growth in a high-strength aluminum alloy. Acta Mater 2007;55(6):1975–84.
[49] Yi JZ, Gao YX, Lee PD, Lindley TC. Effect of Fe-content on fatigue crack initiation and propagation in a cast aluminum–silicon alloy (A356–T6). Mater Sci Eng, A 2004;386(1):396–407.
[50] Goswami R, Feng CR, Qadri SB, Pande CS. Fatigue-Assisted grain growth in Al alloys. Sci Rep 2017;7(1):1–7.
[51] Meyers MA, Mishra A, Benson DJ. Mechanical properties of nanocrystalline materials. Prog Mater Sci 2006;51(4):427–556.